Modeling and Comparative Control Analysis of a Quadrotor UAV: PD, LQR, and LQI Approaches*

Berat Umut Ipek[1], Aylin Bakkal[2], Merve Uzunoglu[3], and Ibrahim Aliskan[4]

***Abstract*— In this study, the position and attitude control dynamics of a quadrotor UAV are investigated using a nonlinear Newton-Euler model, with a primary focus on the comparative performance analysis of PD, LQR, and LQI controllers within the context of current literature. The LQI controller utilizes augmented integral states, and its asymptotic stability is confirmed via a Lyapunov argument derived from the algebraic Riccati equation. The core contribution is a rigorous, three-scenario quantitative benchmark, evaluating helical trajectory tracking, wind disturbance rejection, and agile planar maneuvering, to systematically analyze controller performance with fully reproducible, analytically justified tuning. Results show LQI reduces tracking error by $\approx 90\%$ versus PD under wind disturbances. Limitations, including the absence of hardware validation, are explicitly discussed.**

I. INTRODUCTION

Quadrotors are underactuated, nonlinear systems widely used in autonomous applications. Their control remains an active research area [1], [2]. Early PD/PID designs [3] suffer from steady-state offsets under disturbances. LQR provides optimal state feedback with stability guarantees [4], while LQI adds integral action for zero-steady-state-error tracking [5]. Recent advances include MPC-LPV and LQI-LPV approaches for variable disturbances and parameter-varying dynamics [6]. Despite the rich literature, a systematic quantitative comparison of PD, LQR, and LQI under complex 3D trajectories and severe disturbances remains scarce. This paper makes three explicit contributions:

1) Quantitative benchmark across three distinct scenarios, isolating the effect of integral action on steady-state and transient performance.
2) Formal stability analysis: closed-form Bode margins for PD; Lyapunov-based proof for LQR/LQI via the Riccati equation.
3) Reproducible tuning: all gains derived analytically or via Bryson's rule with explicit justification.

This benchmark serves as an accessible baseline before advancing to strategies such as MPC or adaptive control. The paper is organized as follows: Section II presents the kinematic and dynamic model. Section III details the theoretical development of the controller architectures, with a focus on the augmented LQI design. Section IV presents the simulation results, and Section V concludes the study.

*This work was supported by TUBITAK under the grant number of 2209A - 1919B012418947 and Yildiz Technical University under the grant number of FLO-2025-7435.

[1]Berat Umut Ipek is with Department of Control and Automation Engineering, Yildiz Technical University, Istanbul, Türkiye umut.ipek@std.yildiz.edu.tr

[2]Aylin Bakkal is with Department of Control and Automation Engineering, Yildiz Technical University, Istanbul, Türkiye aylin.bakkal@std.yildiz.edu.tr

[3]Merve Uzunoglu is with Department of Control and Automation Engineering, Yildiz Technical University, Istanbul, Türkiye merve.uzunoglu@std.yildiz.edu.tr

[4]Ibrahim Aliskan is with Department of Control and Automation Engineering, Yildiz Technical University, Istanbul, Türkiye ialiskan@yildiz.edu.tr

II. QUADCOPTER MODELLING

A. Nonlinear Dynamic Model

Quadrotor UAVs are nonlinear, multivariable, and underactuated systems with strong coupling between translational and rotational dynamics. The modeling procedure is based on the Newton-Euler formulation and incorporates rigid-body dynamics, Euler-angle-based attitude representation, and rotor-generated forces and moments [1], [7].

B. Reference Frames and Kinematics

The UAV system is illustrated in Fig. 1. The motion of the quadrotor is described using two coordinate frames: an inertial frame fixed to Earth and a body-fixed frame attached to the vehicle's center of mass. The position is defined as $p = [x, y, z]^T$, and the orientation is represented by Euler angles $\eta = [\phi, \theta, \psi]^T$ (roll, pitch, yaw). Adopting the ZYX convention, the rotation matrix $R(\phi, \theta, \psi)$ mapping vectors from the body frame to the inertial frame is expressed as:

$$R = \begin{bmatrix} c\theta c\psi & s\phi s\theta c\psi - c\phi s\psi & c\phi s\theta c\psi + s\phi s\psi \\ c\theta s\psi & s\phi s\theta s\psi + c\phi c\psi & c\phi s\theta s\psi - s\phi c\psi \\ -s\theta & s\phi c\theta & c\phi c\theta \end{bmatrix} \quad (1)$$

where c and s denote cos and sin, respectively.

The linear velocity in the inertial frame is related to the body frame velocity v_b through $\dot{p} = Rv_b$. Similarly, the angular velocity vector in the body frame $\omega = [p, q, r]^T$ is related to the Euler angle rates by the transformation matrix:

$$\omega = \begin{bmatrix} 1 & 0 & -\sin\theta \\ 0 & \cos\phi & \sin\phi\cos\theta \\ 0 & -\sin\phi & \cos\phi\cos\theta \end{bmatrix} \begin{bmatrix} \dot{\phi} \\ \dot{\theta} \\ \dot{\psi} \end{bmatrix} \quad (2)$$

The Euler-angle representation is valid for small to moderate pitch angles, which is consistent with the operating envelope assumed in the subsequent controller design and linearization procedures.

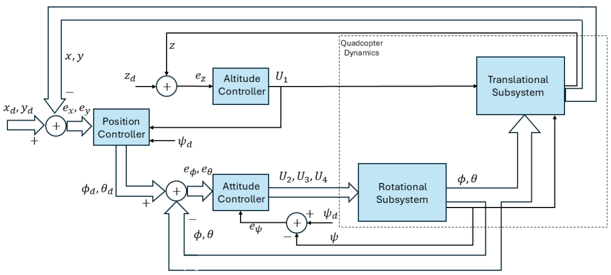

Fig. 1. Quadrotor UAV Motion and Coordinate Systems.

C. Translational and Rotational Dynamics

The translational dynamics are derived from Newton's second law. The total thrust U_1 acts along the body z-axis [8]. The equations of motion in the inertial frame are:

$$\ddot{x} = \frac{U_1}{m}(\cos\phi \sin\theta \cos\psi + \sin\phi \sin\psi) \tag{3}$$

$$\ddot{y} = \frac{U_1}{m}(\cos\phi \sin\theta \sin\psi - \sin\phi \cos\psi) \tag{4}$$

$$\ddot{z} = \frac{U_1}{m}(\cos\phi \cos\theta) - g \tag{5}$$

Here, m is the mass of the UAV and g is the gravity. The rotational dynamics are derived using Euler's rotational equations $I\dot{\omega} + \omega \times (I\omega) = \tau$. The expanded form is:

$$\dot{p} = \frac{I_{yy} - I_{zz}}{I_{xx}} qr + \frac{U_2}{I_{xx}} \tag{6}$$

$$\dot{q} = \frac{I_{zz} - I_{xx}}{I_{yy}} pr + \frac{U_3}{I_{yy}} \tag{7}$$

$$\dot{r} = \frac{I_{xx} - I_{yy}}{I_{zz}} pq + \frac{U_4}{I_{zz}} \tag{8}$$

The thrust force is first expressed in the body-fixed frame and then transformed into the inertial frame using the rotation matrix $R(\phi, \theta, \psi)$, resulting in the translational dynamics given in Eqs. (3)–(5).

D. Actuator Forces and Control Inputs

Each rotor generates a thrust force $f_i = k_f \Omega_i^2$ and a reaction torque $\tau_i = k_m \Omega_i^2$ where $i \in \{1, \ldots, 4\}$. The control inputs are defined as:

$$\begin{bmatrix} U_1 \\ U_2 \\ U_3 \\ U_4 \end{bmatrix} = \begin{bmatrix} k_f & k_f & k_f & k_f \\ 0 & k_f l & 0 & -k_f l \\ -k_f l & 0 & k_f l & 0 \\ k_m & -k_m & k_m & -k_m \end{bmatrix} \begin{bmatrix} \Omega_1^2 \\ \Omega_2^2 \\ \Omega_3^2 \\ \Omega_4^2 \end{bmatrix} \tag{9}$$

where l denotes arm length, k_f is the force constant, k_m is the torque constant and Ω_i represents the angular velocity of the i-th rotor.

III. CONTROL DESIGN AND STABILITY

In this section, the development of PD, LQR, and LQI control strategies is presented. The objective is to evaluate the theoretical framework and stability properties prior to simulation.

A. PD Controller Development

The PD controller is designed independently for each axis, treating the quadcopter dynamics as decoupled Single-Input Single-Output (SISO) systems under the small-angle assumption ($\sin(\phi) \approx \phi$) [3]. The transfer functions for the attitude dynamics are approximated as double integrators. For example, the roll angle dynamics linearized about hover equilibrium ($\phi = \theta = 0$, $U_1 = mg$) are [8]:

$$G_\phi(s) = \frac{\phi(s)}{U_2(s)} = \frac{1}{I_{xx} s^2} \tag{10}$$

The control law minimizes the error $e(t) = r(t) - y(t)$:

$$u(t) = K_p e(t) + K_d \frac{de(t)}{dt} \tag{11}$$

Derivative action is required to introduce damping to the marginally stable double-integrator system. Stability is guaranteed by the Routh-Hurwitz criterion for $K_p, K_d > 0$. The gains are computed analytically: $K_p = I_{xx}\omega_n^2$, $K_d = 2\zeta\omega_n I_{xx}$ [3]. Inner loop (roll/pitch): $\omega_n = 6\ rad/s$, $\zeta = 0.707$; yaw: $\omega_n = 4\ rad/s$; position: $\omega_n = 1.5\ rad/s$, $\zeta = 0.8$ (one-decade separation from inner loop). To prevent high-frequency noise amplification and ensure physical realizability, the derivative term of the PD controller is modified with a first-order low-pass filter as $K_d \frac{Ns}{s+N}$, where $N = 100$ represents the filter bandwidth. Bode analysis confirms phase margin 63.6° at 36.4 rad/s and infinite gain margin.

B. LQR Controller Development

To mitigate trajectory tracking errors caused by axis coupling, an LQR is developed using the full 12-state representation. The system is linearized about the hover equilibrium point ($\phi = \theta = \psi = 0$, $U_1 = mg$), yielding the state-space model $\dot{x} = Ax + Bu$. The LQR minimizes the cost function:

$$J = \int_0^\infty (x^T Q x + u^T R u) dt \tag{12}$$

The Riccati equation yields $P > 0$ satisfying $A_{cl}^T P + P A_{cl} = -(Q + K^T R K)$, where $A_{cl} = A - BK_{lqr}$. Then $V(x) = x^T P x$ is a Lyapunov function with $\dot{V} < 0$, proving asymptotic stability [4].

C. LQI Controller Development

Standard LQR guarantees stability but does not inherently eliminate steady-state error under constant external disturbances or model uncertainties. To overcome this, a Linear Quadratic Integral (LQI) controller is proposed [5].

1) Augmented System Formulation: The control objective is to ensure that the output $y(t)$ tracks the reference $r(t)$ asymptotically. The tracking error is defined as:

$$e(t) = r(t) - y(t) = r(t) - Cx(t) \tag{13}$$

To eliminate this error, an integral state vector x_i is introduced such that $\dot{x}_i(t) = e(t)$. We define a new augmented state vector $z(t)$ combining the system states and the integral states [4]:

$$z(t) = \begin{bmatrix} x(t) \\ x_i(t) \end{bmatrix} \tag{14}$$

The output vector is defined as $y = [x\ y\ z\ \psi]^T$, and the corresponding rows of the output matrix C are selected accordingly. Integral states $\dot{x}_i = r - Cx$ are augmented for x, y, z, ψ channels. The augmented system $z = [x^T, x_i^T]^T$ is:

$$\dot{z} = \tilde{A}z + \tilde{B}u, \quad \tilde{A} = \begin{bmatrix} A & 0 \\ -C & 0 \end{bmatrix}, \quad \tilde{B} = \begin{bmatrix} B \\ 0 \end{bmatrix} \tag{15}$$

2) Optimal Control Law: The LQI control input is determined by minimizing the infinite-horizon cost $J = \int_0^\infty (z^T Q_{aug} z + u^T R u) dt$ [4]. Using the augmented weight $Q_{aug} = \mathrm{diag}(Q_x, Q_i)$, where $Q_i > 0$ penalizes the integral error, LQR applied to $(\tilde{A}, \tilde{B})$ yields $\tilde{P} > 0$. The optimal feedback control law simplifies to $u = -K_{aug} z = -K_x x - K_i x_i$. The Lyapunov function $V = z^T \tilde{P} z$ confirms asymptotic stability, shifting integrator poles to stable locations. By the Internal Model Principle, $e(t) \to 0$ as $t \to \infty$ for constant disturbances [6]. Remark: The small residual LQI error ($\approx 0.05\ m$) on the helical trajectory results from the linearization-induced model mismatch, not a flaw in the integral mechanism; for constant setpoints, near-exact zero error is achieved.

3) Weight Selection: Bryson's rule is the starting point. The z-velocity is penalized heavily ($Q_{6,6} = 15$) to prevent altitude overshoot. The altitude integral weight $Q_{i,z} = 600$ is twice the horizontal channels ($Q_{i,x} = Q_{i,y} = 300$). The input weight $R = 0.1I$ for LQI (vs. $R = I$ for LQR) enables more aggressive disturbance rejection; actuator saturation was verified across all scenarios. Full gains are in Table 2.

IV. Simulation and Performance Analysis

In this section, the performance of the proposed PD, LQR, and LQI controllers is evaluated through numerical simulations. The simulations were conducted using the nonlinear dynamic model derived in Section II, with a sampling time of $T_s = 0.005$ s.

A. System Parameters

The physical parameters of the quadrotor platform used in this study are listed in Table I. These values were utilized to compute the system matrices A and B.

TABLE I

Physical Parameters of the Quadrotor

Symbol	Description	Value	Unit
m	Mass	0.65	kg
l	Arm Length	0.23	m
I_{xx}, I_{yy}	Roll/Pitch Inertia	0.0075	kg·m^2
I_{zz}	Yaw Inertia	0.0130	kg·m^2
J_r	Rotor Inertia	6.0×10^{-5}	kg·m^2
k_f	Thrust Coeff.	3.13×10^{-5}	N/(rad/s)^2
k_m	Drag Coeff.	7.5×10^{-7}	N·m/(rad/s)^2
g	Gravity	9.81	m/s^2

B. Controller Tuning and Stability Analysis

The control parameters were tuned based on the principle of time-scale separation for the PD controller and quadratic cost minimization for the optimal controllers.

1) PD Controller Tuning: The PD gains were calculated analytically to meet specific natural frequency (ω_n) and damping ratio (ζ) targets.

- **Inner Loop (Attitude):** The Roll and Pitch axes were tuned to be aggressive ($\omega_n = 6$ rad/s) for fast stabilization. The Yaw axis was tuned with a slightly slower response ($\omega_n = 4$ rad/s).
- **Outer Loop (Position):** To prevent interference with the inner loop, the position control was designed to be slower ($\omega_n = 1.5$ rad/s, $\zeta = 0.8$).
- **Altitude (Z):** High gains were selected to counteract gravity effectively.

Fig. 2 illustrates the Bode diagram of the compensated dynamics, confirming the stability margins.

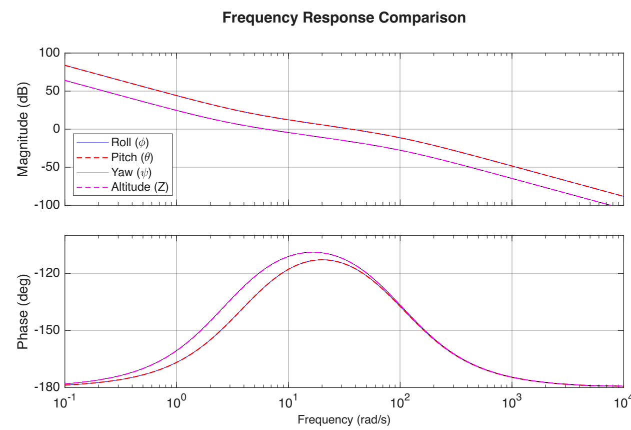

Fig. 2. Bode plot of the compensated dynamics. The phase and gain margins confirm the stability of the inner control loop.

2) LQR and LQI Tuning: For the optimal controllers, the weighting matrices were selected to prioritize position tracking accuracy. In the LQR design, the Z-axis velocity is heavily penalized ($Q_{6,6} = 15$) to prevent altitude overshoot.

For the LQI controller, the state weights (Q_x) were kept consistent with the LQR design. However, to eliminate steady-state errors rapidly, high penalties were assigned to the integral states (Q_i), particularly for the altitude ($Q_{i,z} = 600$). Additionally, the input weighting matrix R was reduced to 0.1 for LQI (compared to 1.0 in LQR) to allow for more aggressive control actions. The resulting parameters are summarized in Table II.

C. Simulation Scenario 1: Unperturbed Path Tracking

In the first simulation scenario, the quadrotor is tasked with tracking a helical (spiral) trajectory under ideal conditions, with no external disturbances applied. This scenario evaluates the baseline tracking performance and the ability of the controllers to handle coupled 3D motion.

The reference trajectory is defined as a climbing spiral, requiring simultaneous coordination of roll, pitch, yaw, and throttle commands.

1) 3D Trajectory Tracking Performance: Fig. 3 presents the 3D trajectory tracking results for the PD, LQR, and LQI controllers.

TABLE II
CONTROLLER GAIN PARAMETERS

Method	Loop/Term	Parameter	Value
PD	Inner Loop (ϕ, θ)	K_p, K_d	1.17, 0.277
	Yaw (ψ)	K_p, K_d	0.208, 0.074
	Altitude (z)	K_p, K_d	10.40, 3.68
	Position (x, y)	K_p, K_d	1.46, 1.56
LQR	State Weight	Q	$\text{diag}(5,5,1,5,5,15,\dots)$
	Input Weight	R	$\text{diag}(1,1,1,1)$
LQI	State Weight	Q_x	Same as LQR
	Integ. Weight	Q_i	$\text{diag}(300,300,600,300)$
	Input Weight	R	$\text{diag}(0.1,0.1,0.1,0.1)$

As observed, all three controllers successfully stabilize the vehicle and follow the general shape of the spiral path. However, a distinct difference in tracking accuracy is visible. The LQI controller (green line) overlaps almost perfectly with the reference trajectory (black dashed line), indicating superior performance. In contrast, both the PD (orange) and standard LQR (blue) controllers exhibit a noticeable steady-state offset, trailing the reference path throughout the simulation.

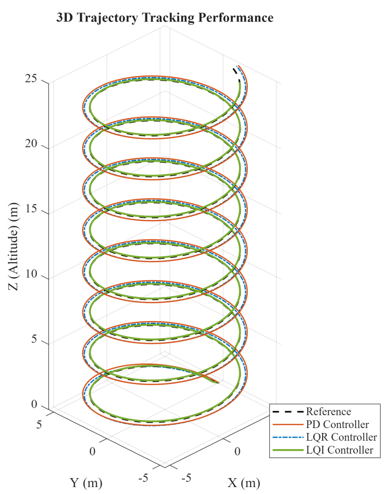

Fig. 3. 3D Trajectory Tracking Performance (Scenario 1). While all controllers maintain stability, LQI demonstrates the tightest adherence to the reference path.

2) Tracking Error Analysis: To quantify the tracking accuracy independent of time, the Tracking Error metric is analyzed. This metric represents the shortest Euclidean distance between the drone's position and the reference path.

Fig. 4 illustrates the tracking error over time. The results confirm the visual observations from the 3D plot:

- **PD Controller:** Settles at a constant tracking error of approximately 0.46 m. Since the PD controller lacks integral action, it cannot fully eliminate the error caused by the constantly changing operating point of the spiral trajectory (Type 0 system behavior for ramp-like inputs).
- **LQR Controller:** Shows a steady-state error of approximately 0.36 m. Although better than PD, the standard LQR also lacks the integral action required to achieve zero steady-state error in this trajectory tracking task.
- **LQI Controller:** Demonstrates superior performance with a tracking error converging to approximately 0.05 m. The augmented integral states in the LQI design effectively compensate for the tracking deviations, reducing the error by nearly 90% compared to the PD controller.

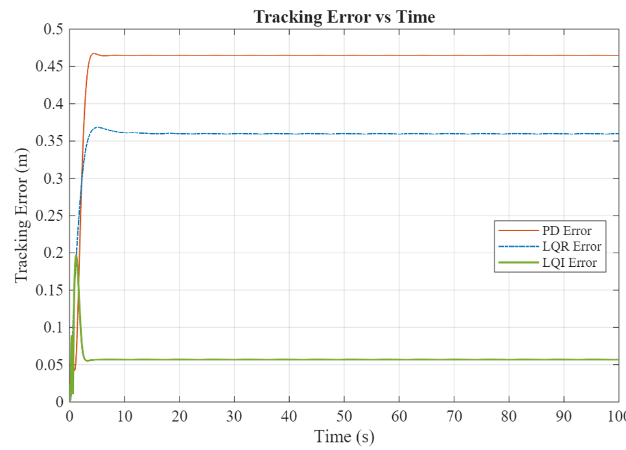

Fig. 4. Tracking Error Analysis. LQI minimizes the geometric deviation significantly compared to PD and LQR.

Table III summarizes the numerical performance metrics for Scenario 1.

TABLE III
PERFORMANCE COMPARISON (SCENARIO 1)

Controller	Mean Tracking Error (m)
PD	0.465
LQR	0.360
LQI	**0.056**

D. Simulation Scenario 2: Disturbance Rejection Performance

In this scenario, the robustness of the control architectures is evaluated under severe environmental disturbances. While the quadrotor tracks the spiral trajectory shown in Fig. 5, a continuous wind gust is applied to simulate a high-resistance flight condition.

1) Disturbance Parameters: The disturbance is modeled as a constant force step input with the following characteristics:

- **Timing:** The disturbance is active between $t = 15$ s and $t = 45$ s (indicated by the grey shaded regions in the time-response plots).
- **Magnitude:** A force of 2.5 N is applied simultaneously in both the $+X$ and $-Y$ axes.

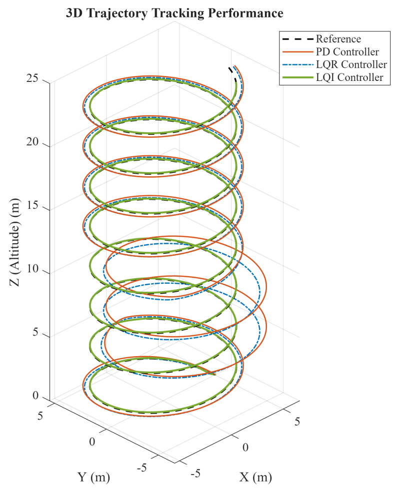

Fig. 5. 3D Spiral Trajectory Tracking. The vehicle performs a climbing maneuver while subject to external wind disturbances.

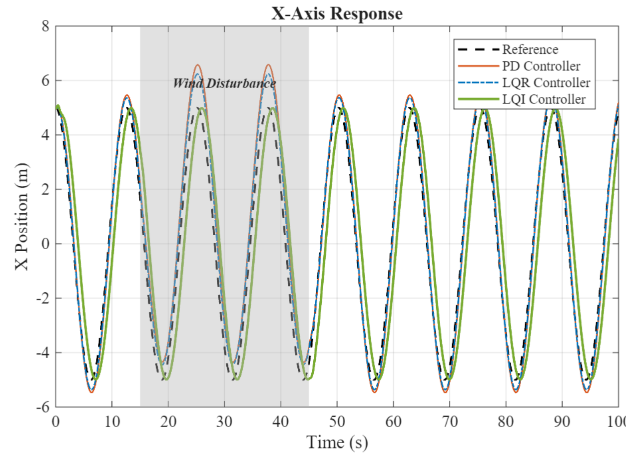

Fig. 6. X-Axis Response under Wind Disturbance. The LQI controller eliminates the drift caused by the wind, while PD and LQR sustain a steady offset.

- **Physical Interpretation:** This represents a significant aerodynamic loading condition for the 0.65 kg quadrotor.

2) Transient Response Analysis: The time-domain responses of the quadrotor along the X and Y axes are presented in Fig. 6 and Fig. 7, respectively.

Upon the onset of the disturbance at $t = 15$ s, all controllers experience an initial deviation. However, their recovery characteristics differ fundamentally:

- **PD and LQR (Steady-State Offset):** Both the PD (orange line) and LQR (blue line) controllers exhibit a permanent steady-state error (drift) as long as the wind persists. Since these controllers lack integral action, they require a non-zero position error to generate the necessary counter-thrust to balance the external wind force. This results in the vehicle tracking a "shifted" trajectory parallel to the reference.
- **LQI (Disturbance Rejection):** The LQI controller (green line) successfully rejects the disturbance. The integral states rapidly accumulate the error caused by the wind and automatically adjust the control effort. As seen in the figures, the LQI controller forces the vehicle back to the reference trajectory within a few seconds, even while the 2.5 N wind force is still active.

3) Tracking Error Analysis: The overall tracking accuracy is quantified using the Absolute Tracking Error metric, as shown in Fig. 8.

During the disturbance interval, the PD controller suffers the largest deviation, with errors peaking at approximately 2.05 m. The LQR controller improves slightly, but still maintains a high error of ≈ 1.65 m. In contrast, the LQI controller suppresses the peak error significantly and converges to a near-zero error state (≈ 0.06 m). This demonstrates that the LQI approach reduces the tracking deviation by over 90% compared to the PD controller under heavy wind loads.

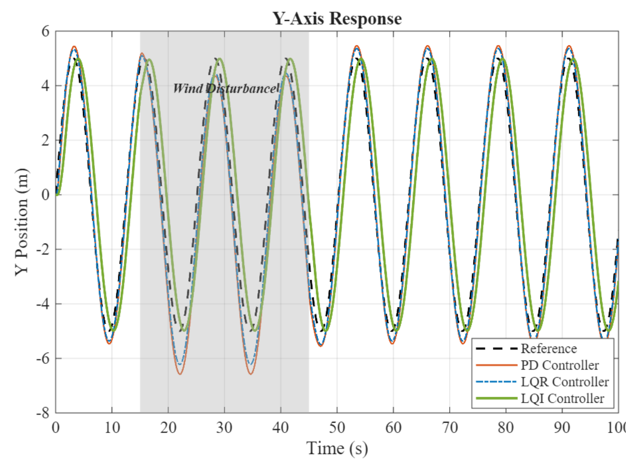

Fig. 7. Y-Axis Response under Wind Disturbance. The grey zone indicates the active disturbance period ($t \in [15, 45]$ s).

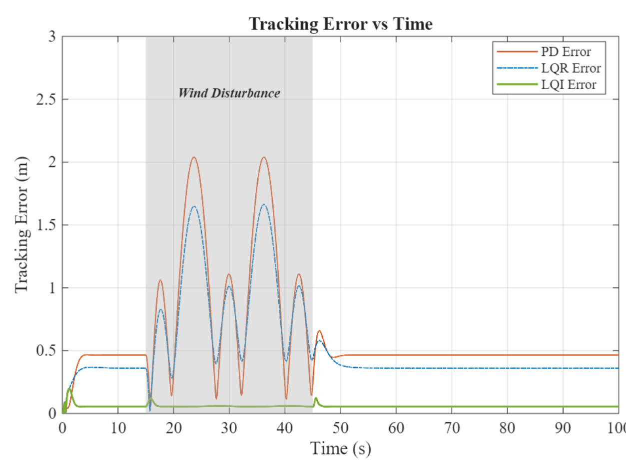

Fig. 8. Tracking Error vs. Time. The LQI controller maintains sub-10cm accuracy after the transient phase, proving its robustness.

E. Simulation Scenario 3: Complex Planar Trajectory (Agility Test)

In the final simulation scenario, the quadrotor is tasked with tracking a complex 2D planar trajectory formed by the acronym of the institution. This path is specifically chosen to evaluate the controller's performance during aggressive maneuvers involving sharp turns and sudden directional changes. This path contains discontinuous velocity profiles at the vertices of the letters, and these serve as a stress test for the transient response of the control loops.

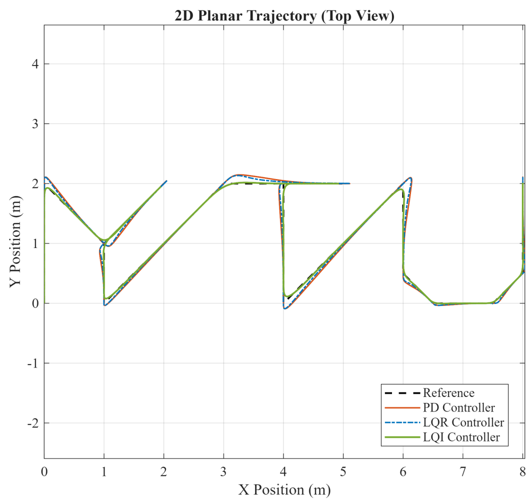

Fig. 9. 2D Planar Trajectory Tracking (Top View). The path consists of sharp turns representing the institution's acronym, testing the agility of the controllers.

1) Performance at Sharp Corners: As illustrated in Fig. 9, the tracking performance varies significantly at the critical turning points:

- The PD (orange line) and LQR controller (blue line) exhibit noticeable overshoot and lag at the sharp corners. Due to the lack of integral action to accumulate error history, they tend to "cut corners" and react slower to sudden changes in the reference trajectory.
- The LQI controller (green line) demonstrates superior agility. By effectively processing the tracking error through its integral states, it generates the necessary control torque more rapidly. This allows the quadrotor to adhere strictly to the reference path, even at the vertices where the trajectory direction changes abruptly.

This scenario confirms that the proposed LQI architecture is not only robust against environmental disturbances (as shown in Scenario 2) but is also capable of precise tracking during agile maneuvering tasks.

F. Discussion and Limitations

The results confirm that integral action is essential for steady-state error elimination and disturbance rejection. The following limitations should be noted: (1) Simulation only: HIL and physical flight tests are needed; actuator delays, sensor noise, and flexible dynamics are not modeled. (2) Linearization mismatch: performance may degrade under large-angle maneuvers; gain scheduling or MPC-LPV [6] can mitigate this. (3) Scope: MPC, H_∞, and adaptive methods are out of scope but represent natural extensions.

V. CONCLUSIONS

This paper presented a comparative analysis of PD, LQR, and LQI control strategies for a quadrotor UAV modeled via the Newton-Euler formalism. The controllers were evaluated through comprehensive simulations, including helical trajectory tracking and disturbance rejection. The key findings are summarized as follows:

- The PD controller ensured stability for basic maneuvers but suffered from significant steady-state error (0.46 m) during trajectory tracking and failed to compensate for wind disturbances, resulting in a drift exceeding 2.0 m.
- The LQR controller improved transient response and reduced tracking error compared to PD. However, lacking integral action, it could not entirely eliminate steady-state offsets, particularly under aerodynamic loading.
- The LQI controller demonstrated superior performance by augmenting integral states. It successfully eliminated steady-state errors, achieving an accuracy of approximately 0.05 m, and effectively rejected external disturbances, reducing tracking error by over 90% compared to PD.

These results confirm that while linear methods are effective for stabilization, integral action (as in LQI) is critical for high-precision flight in the presence of environmental disturbances. Future work will focus on experimental validation and the implementation of adaptive control techniques to handle payload variations.

REFERENCES

[1] S. Bouabdallah, P. Murrieri, and R. Siegwart, Design and control of an indoor micro quadrotor, in Proc. IEEE Int. Conf. Robot. Autom. (ICRA), pp. 4393–4398, 2004.

[2] R. Mahony, V. Kumar, and P. Corke, "Multirotor aerial vehicles: Modeling, estimation, and control of quadrotor," IEEE Robot. Autom. Mag., vol. 19, no. 3, pp. 20–32, 2012.

[3] K. Ogata, Modern Control Engineering, 5th ed. Upper Saddle River, NJ, USA: Prentice Hall, 2010.

[4] B. D. O. Anderson and J. B. Moore, Optimal Control: Linear Quadratic Methods. Englewood Cliffs, NJ, USA: Prentice-Hall, 1990.

[5] A. R. Merheb, H. Noura, and F. Bateman, Design and implementation of LQR and LQI controller for a quadrotor, in Proc. IEEE Int. Conf. Syst. Control (ICSC), pp. 1–6, 2015.

[6] R. H. Chowdhury, A. I. Ferdous, A. Hossain, and K. A. Rahman, "Enhancing trajectory tracking of quadrotor using feedback linearization with MPC-LPV and LQI-LPV under variable disturbances," in Proc. IEEE RAAICON, pp. 133-138, 2024.

[7] T. Luukkonen, "Modelling and control of quadcopter," Independent research project in applied mathematics, Aalto University, Espoo, Finland, 2011.

[8] A. Demiryurek, Modeling and Control of a Quadrotor, M.S. thesis, Dept. Elect. Electron. Eng., Hacettepe Univ., Ankara, Turkey, 2018.

[9] N. Koksal, H. An, and B. Fidan, "Adaptive linear quadratic tracking control of a quadrotor UAV based on IMU sensor data fusion," Sensors, vol. 19, no. 1, p. 46, 2019.

[10] T. Bresciani, "Modelling, identification and control of a quadrotor helicopter," M.S. thesis, Dept. Autom. Control, Lund Univ., Lund, Sweden, 2008.

[11] S. Di Cairano and A. Bemporad, "Control design for UAV quadrotors via embedded model control," IEEE Transactions on Control Systems Technology, vol. 27, no. 4, pp. 1684–1691, 2019.